GDCh

Research Article

Angewandte
Chemie
International Edition
www.angewandte.org

Polymer Chemistry | Hot Paper

4D Printing of Liquid Crystal Emulsions for Smart Structures with Multiple Functionalities

Alberto Concellón,* Philipp Mainik, Clara Vazquez-Martel, Cristina Álvarez-Solana, and Eva Blasco*

Abstract: 3D printing, and more recently 4D printing, has emerged as a transformative technology for fabricating structures with complex geometries and responsive properties. However, employing functional colloidal solutions as inks for printing remains unexplored. In this work, we present a novel and versatile 4D printing approach for fabricating functional and complex-shaped objects using polymerizable liquid crystal (LC) emulsion droplets. Leveraging a digital light processing (DLP) 3D printing technique, we achieve rapid production of intricate 3D geometries with high resolution. The printed structures retain the LC ordering from the precursor droplets, imparting the final objects with shape memory properties, including shape fixation and recovery upon heating or light exposure. Light-responsive behavior is introduced post-printing by embedding an azo dye into the 3D structures. Additionally, we explore the potential to create intrinsically porous 3D structures by selectively removing non-reactive components from the printed geometries, adding an extra level of functionality to the printed objects. Furthermore, we incorporate chiral nematic LCs into the emulsion droplets, producing 3D objects with tunable reflective properties. To our knowledge, this is the first example of DLP 3D printing with emulsions, offering an effective and versatile pathway for developing 4D-printed materials with potential applications in optics, robotics, microfluidics, and biomedicine.

Introduction

In recent years, three-dimensional (3D) printing, also known as additive manufacturing, has revolutionized the production of complex objects, facilitating the creation of intricate 3D structures that are challenging to produce using conventional technologies such as subtractive manufacturing or molding.[1] The digital nature of additive manufacturing allows for the rapid transition from computer-aided designs to physical objects, significantly reducing development time and accelerating the transformation of ideas into products. This innovation has had a significant impact across various fields, including healthcare, microfluidics, aerospace, automotive, and robotics.[2] Traditional light-based 3D printing materials, often referred to as inks or resins, are typically composed of thermoplastics, resulting in rigid and static objects. However, the emergence of four-dimensional (4D) printing has expanded these capabilities by introducing smart materials that can change shape or other properties over time in response to external stimuli.[3] For this purpose, various strategies have been explored, including the use of responsive polymers such as hydrogels,[4] shape memory polymers,[5] composites,[6] and liquid crystal elastomers.[7]

One successful strategy to enhance the performance of responsive polymers is embedding functional inclusions such as droplets, bubbles, or (nano)particles within the polymer matrix.[8] These inclusions can significantly improve properties such as actuation capabilities, electrical conductivity, or mechanical strength. For instance, incorporating liquid metal droplets into an elastic polymer matrix can enhance the thermal and electrical conductivity of the polymeric actuators.[9] One promising approach involves dispersing active colloids, such as nanoparticles or emulsion droplets,

[*] Dr. A. Concellón, C. Álvarez-Solana
Instituto de Nanociencia y Materiales de Aragón (INMA)
CSIC-Universidad de Zaragoza
50009 Zaragoza, Spain
E-mail: aconcellon@unizar.es

Dr. A. Concellón, C. Álvarez-Solana
Departamento de Química Orgánica
Universidad de Zaragoza
50009 Zaragoza, Spain

P. Mainik, C. Vazquez-Martel, Prof. Dr. E. Blasco
Institute for Molecular Systems Engineering and Advanced Materials (IMSEAM)
Heidelberg University
69120 Heidelberg, Germany
E-mail: eva.blasco@uni-heidelberg.de

P. Mainik, C. Vazquez-Martel, Prof. Dr. E. Blasco
Organic Chemistry Institute (OCI)
Heidelberg University
69120 Heidelberg, Germany

in a polymer solution that can be readily printed into functional 3D structures.[10] However, innovative strategies are still needed to design inks containing colloidal systems with tailored functionalities, which can be readily manufactured into complex 3D objects. In fact, the use of functional colloidal solutions as inks for 3D printing has not yet been fully realized, presenting an exciting opportunity for further research and development in the field.

Among the various functional colloidal systems, liquid crystal (LC) emulsions are particularly promising due to their unique stimuli-responsive and adaptive characteristics. LCs are self-assembled materials that combine distinctive anisotropic properties with liquid-like fluidity.[11] Nanostructured LC phases, such as smectic, columnar, and cubic phases, have been developed through diverse molecular designs, enabling the creation of functional materials for applications in optoelectronics, energy storage, separation technologies, sensing, among others.[12] The introduction of chirality into LC nanostructures has further been shown to enhance electro-optical and chiro-optical behaviors, as well as to enable ferroelectric properties.[13] While nanostructured LCs have traditionally been processed in solid film slabs, their confinement within emulsion droplets has revealed new and unprecedented properties, making them ideal candidates for smart materials.[14] LC emulsions can be tailored with a variety of internal LC phases, payloads, and interfacial functionalities, expanding their applicability in several advanced technological fields, such as optics, photonics, sensing, and soft robotics.[15] However, LC emulsions face significant limitations due to droplet coalescence, particularly when exposed to air, which compromises their stability and prevents the full realization of their unique functional properties. To address these challenges, we hypothesized that polymerizing LC droplets to form stabilized emulsions, coupled with additive manufacturing techniques such as 3D printing, could enable the fabrication

of complex 3D/4D structures while retaining the distinct and functional characteristics of the LC emulsion droplets.

Herein, we report a novel and versatile 4D printing approach that leverages photopolymerizable liquid crystal (LC) emulsion droplets to fabricate complex-shaped, multifunctional objects (Figure 1). By using digital light processing (DLP) 3D printing, we developed a rapid, high-resolution technique capable of preserving the intrinsic LC arrangement within the emulsion droplets, which remains intact in the final printed 3D structures. This preserved LC ordering endows the objects with inherent shape memory properties, allowing for shape fixation and reversible shape recovery in response to thermal stimulus. To further expand the versatility of the printed structures, light-responsive capabilities were introduced through a post-printing process in which an organic azo dye was embedded within the 3D structures, enabling precise control over shape reconfiguration upon light exposure. We additionally explored the creation of 3D architectures with tunable intrinsic porosity by selectively extracting non-reactive components from the printed objects. Moreover, to achieve tunable reflective properties, chiral nematic LCs were incorporated within the emulsion droplets, resulting in 3D-printed objects with potential photonic capabilities. While various technologies have been employed to create LC-based 3D structures—including direct ink writing, extrusion-based methods, two-photon laser printing, and DLP[16]—this work represents the first demonstration of 3D printing with LC emulsions. Our approach preserves the unique characteristics of the LC emulsion droplets, offering a robust and versatile pathway for developing 4D-printed smart materials with potential applications in adaptive optics, robotics, microfluidics, or biomedicine.

Figure 1. Schematic representation of the preparation of LC emulsion-based inks and the DLP printing process to generating 3D structures maintaining the LC ordering from the precursor droplets.

Results and Discussion

Preparation of Liquid Crystal Emulsions for DLP 3D Printing

To develop LC emulsions-based inks suitable for 3D fabrication via DLP, we first identified the functional emulsion components to be utilized. We selected a LC mixture primarily consisting of 4-cyano-4'pentylbiphenyl (**5CB**), which forms a nematic phase at room temperature, with a nematic-to-isotropic temperature (T_{N-I}) of 35 °C. Additionally, we included 20 wt % of a mesogenic cross-linker (**RM257**) and 1 wt. % of a photoinitiator (**BAPO**) (Figure 1). **BAPO** was chosen due to its appropriate absorption range of 360 to 400 nm, aligning with the DLP curing wavelength of 385 nm. Differential scanning calorimetry (DSC) confirmed that this reactive LC mixture remains in the nematic phase at room temperature and transitions to an isotropic state at 51 °C (Figure S1).

For fabricating photopolymerizable LC emulsions, the reactive LC mixture was dissolved in dichloromethane (DCM) and emulsified, resulting in LC droplets upon DCM evaporation. In particular, we employed a 0.1 wt. % aqueous solution of polyvinyl alcohol (**PVA**) as the continuous phase, leading the LC droplets to adopt a bipolar configuration, as confirmed by polarized-light optical microscopy (POM). In this arrangement, the director of the nematic LC phase aligns parallel to the aqueous interface, generating two point defects, known as boojums, at the droplets' opposing poles. The orientation of the droplets relative to the crossed polarizers of the POM resulted in each droplet displaying a distinct birefringence texture (Figure 2a). We further explored the dynamic alteration of LC internal alignment from bipolar to radial configurations by adding a 0.1 wt. % aqueous solution of sodium dodecyl sulfate (**SDS**) surfactant. This surfactant aligns its alkyl chain perpendicular to the LC/water interface, prompting a similar orientation of the LC director at this interface. Consequently, droplets adopt a radial configuration with a central point defect, displaying the characteristic Maltese cross textures under POM examination (Figure 2a).

Moreover, we demonstrated that both the morphology and internal LC alignment of these LC single droplets can be preserved through photopolymerization, initiated by 365 nm light irradiation for 5 minutes. Upon photopolymeri-
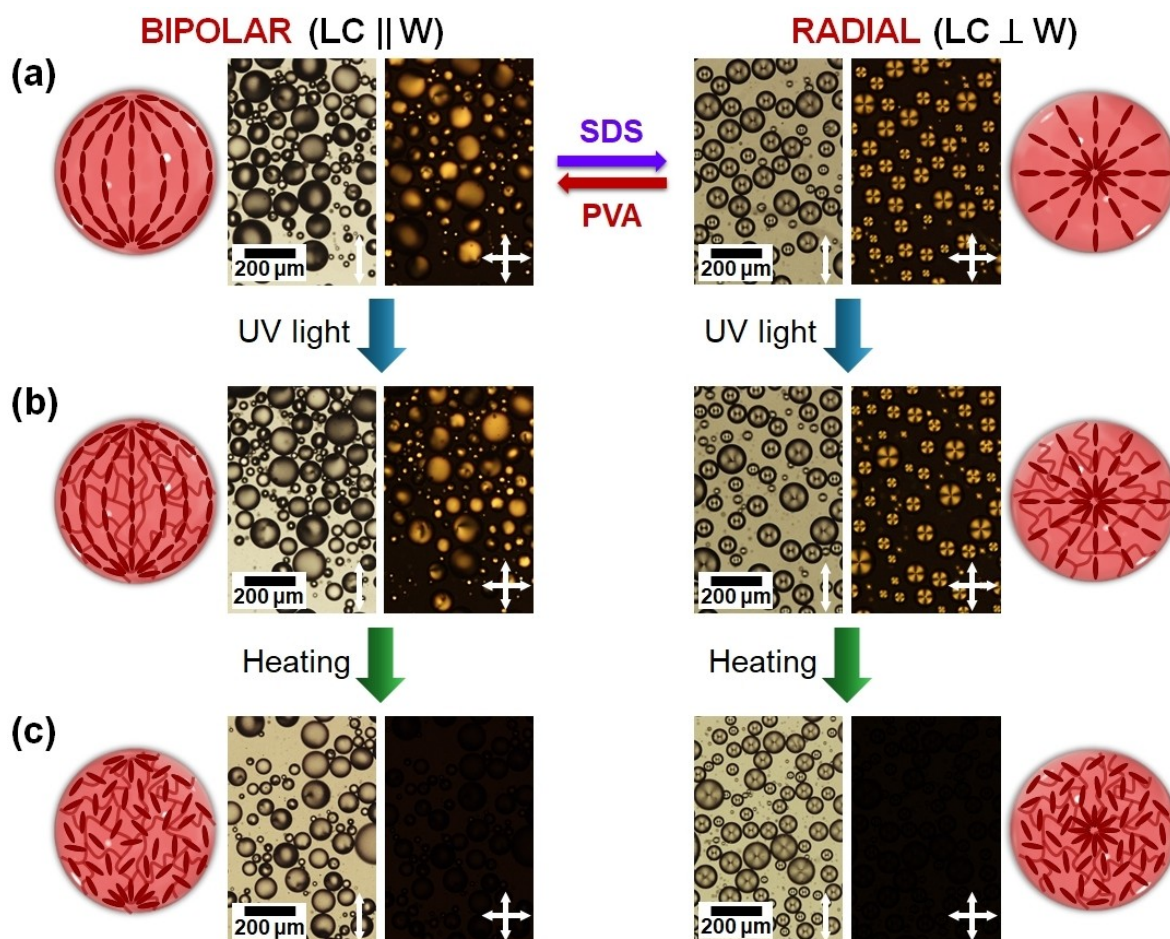
Figure 2. LC emulsion droplets with radial (0.1 wt % **SDS**) or bipolar (0.1 wt % **PVA**) configurations: polarized light optical microscopy images without (left) and with (right) crossed polarizers, and the corresponding representation of the LC director orientation within droplets: **(a)** initial (as prepared), **(b)** after 365 nm light irradiation, **(c)** after heating at 50 °C

zation, it forms a polymer-stabilized nematic LC,[17] where the resultant polymer network templates and stabilizes the nematic LC phase of **5CB**. DSC studies indicated a 2 °C increase in T_{N-I} compared to pure **5CB** (Figure S1). Importantly, POM observations confirmed that the original bipolar or radial internal configurations of the precursor droplets—each displaying either two diametrically opposed defects or a central defect, respectively—remained unaltered in the polymerized LC emulsion droplets (Figure 2b). Heating non-polymerized droplets to the isotropic phase resulted in the disappearance of the birefringence along with the defects present within droplets (Figure S2). Nonetheless, upon heating polymerized droplets above T_{N-I}, we observed the disappearance of the birefringence, whereas defects within the polymerized droplets remained unchanged (Figure 2c). This finding demonstrates the enhanced stability of the polymerized LC emulsion droplets, forming a polymer network that persists above T_{N-I}, and that templates and stabilizes the nematic LC phase of **5CB**. Moreover, the aqueous continuous phase was successfully removed by drop-casting the droplet solution and allowing it to dry at room temperature. This process resulted in the deposition of photopolymerized LC droplets onto solid substrates, preserving their spherical morphology. Interestingly, the photopolymerized droplets retained the internal LC ordering of the pristine droplets, exhibiting radial configurations when **SDS** was used as the surfactant and bipolar configurations when **PVA** was used. This demonstrates that both surfactant solutions can be effectively employed to produce photopolymerizable LC droplets with distinct internal LC alignments (Figure S3).

Fabrication and Characterization of 3D Structures Based on LC Emulsions

The previously prepared emulsion systems were implemented as inks for DLP 3D printing. The DLP printer employed possesses a UV-LED light source ($\lambda = 385$ nm), allowing the photopolymerization and consequently, the creation of objects in the range of millimeters to centimeters via layer-by-layer curing. Direct use of the prepared LC emulsion systems for 3D printing resulted in brittle objects, likely due to insufficient inter-droplet crosslinking. Thus, to enhance stability, an aqueous crosslinker and a water-soluble photoinitiator were added to ensure good printability. Poly(ethylene glycol) diacrylate (**PEGDA**, $M_n = 6.000$ g/mol) was selected as a suitable aqueous-soluble crosslinker that provides droplet-droplet covalent connections, thus ensuring mechanical integrity of the printed structures. Lithium phenyl-2,4,6-trimethylbenzoylphosphinate (**LAP**) was chosen as a suitable water-soluble radical photoinitiator, compatible with the wavelength of the DLP printing system (385 nm). The optimized formulation comprised an aqueous continuous phase containing **PVA** (0.1 wt %) as a surfactant, **PEGDA** (2.5 wt %) as the crosslinker, and **LAP** (0.25 wt %) as the photoinitiator.

Optimal printing parameters, such as irradiation time and intensity, were determined through a series of curing tests using the UV-LED of the DLP 3D printer. Jacobs working curves, derived from the Lambert-Beer law,[18] were calculated at a constant curing intensity of 25 mW/cm² by varying the exposure time from 2 s to 20 s (Figure S4). The critical energy (E_c) necessary for photopolymerization and the penetration depth (D_p) of the ink were found to be 21.5 mJ/cm² and 0.074 mm, respectively. Based on these results, the curing time per layer was established at 10.7 s, with a fixed curing intensity of 25.0 mW/cm², ensuring effective printability with a layer thickness of 100 µm. To demonstrate the versatility of our printing approach, we designed and successfully printed a wide variety of intricate 3D geometries. Effective 3D fabrication in the centimeter range was achieved for simple designs like grids, submarines, and sunflowers, as well as for more complex shapes with significant overhangs, such as roses, rabbits, and infinity rings (Figure 3a). Moreover, all printed structures exhibited smooth transitions between individual cured layers without evidence of over-polymerization, indicating the effective optimization of the printing parameters and excellent performance of the developed ink.

As mentioned above, the non-reactive nematic LC, namely **5CB**, plays a crucial role in the printing process. Although it does not polymerize during printing, the nematic LC molecules facilitate alignment within the droplets that form the ink and enable the formation of a network during printing. This network has enough flexibility for the incorporation of a dye in a subsequent step or for forming a chiral nematic phase (vide infra). The presence of a significant amount of unreactive **5CB** during printing may result in its unwanted removal from inside the printed 3D structure during the development process. We could maintain **5CB** inside the 3D printed structure by rinsing with a solvent in which **5CB** is insoluble, such as a 1:1 (v/v) mixture of ethanol and water, while sonicating the printed structure and subsequently drying it. Infrared (IR) spectroscopy confirmed successful photopolymerization by showing the disappearance of the C=C stretching vibration band at 1635 cm⁻¹ (Figure S5), indicating high conversion in the crosslinking reaction of the acrylate groups. Additionally, it demonstrated that the non-reactive **5CB** was not removed from the printed structures during the washing step, as the intensity of the C≡N stretching band remained unchanged compared to the pristine reactive LC mixture. Further evidence of the presence of **5CB** was provided by DSC studies, which revealed that the printed structures exhibited the nematic-to-isotropic transition (T_{N-I}) of nematic **5CB** with no significant differences in peak area (i.e., enthalpy, in J/g) compared to the pristine reactive LC mixture (Figure S1).

Detailed examination of the distinct features was conducted using a light microscope with crossed polarizers (Figure 3b). The bright-field images revealed a continuous surface with slight roughness due to the close packing of spherical droplets forming the printed structures. POM images confirmed the preservation of the nematic LC phase after printing, as evidenced by the birefringent domains visible in all 3D printed structures under crossed polarizers. Scanning electron microscopy (SEM) further demonstrated
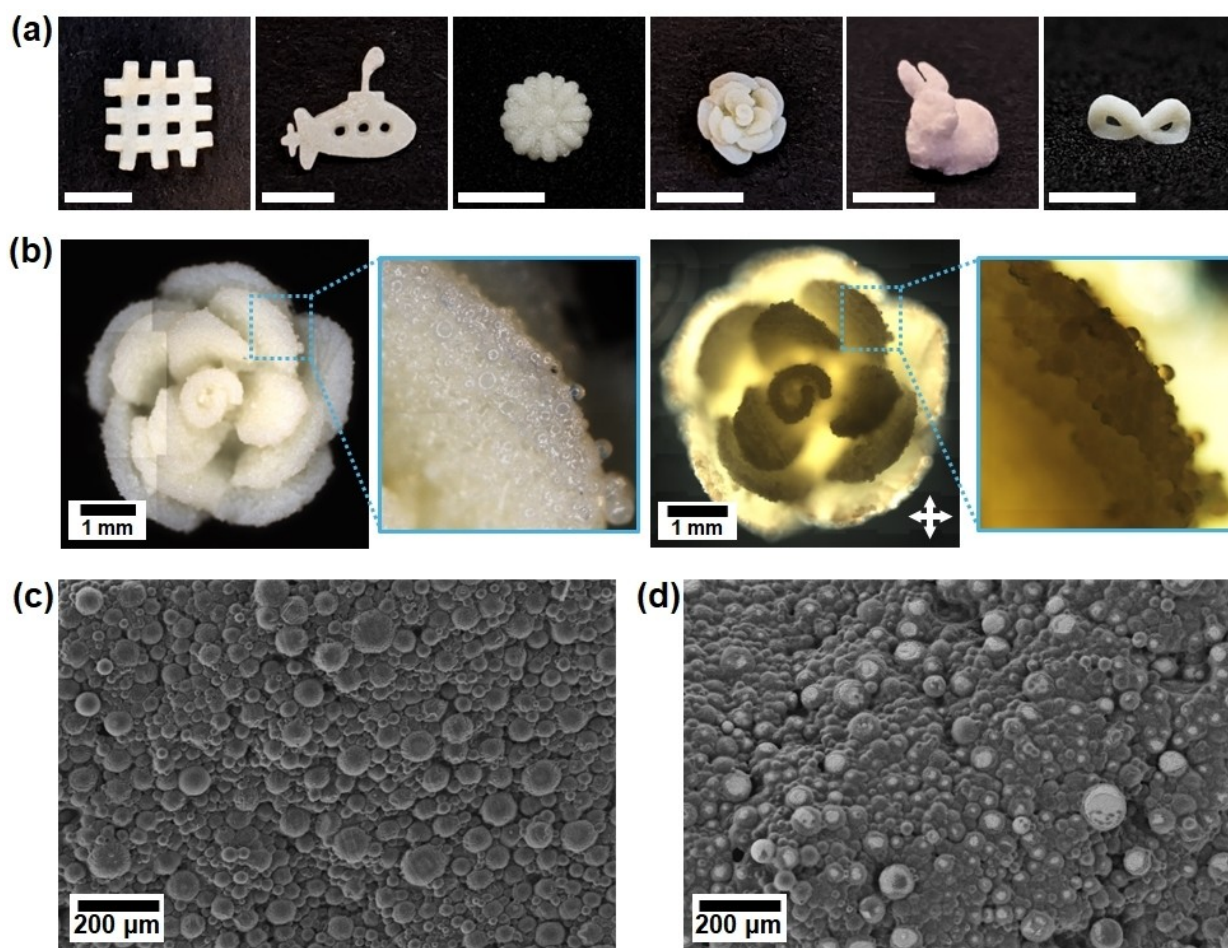
Figure 3. (a) Photographs of the 3D printed structures: grid, submarine, sunflower, rose, rabbit, and infinity ring (from left to right; scale bar: 5 mm). **(b)** Reflection optical microscopy image of a printed structure with (right) and without (left) crossed polarizers. **(c)** Scanning electron microscopy (SEM) image of a printed structure. **(d)** Scanning electron microscopy (SEM) image of a printed structure washed with DCM.

that the 3D printed structures consisted of spherical droplets closely packed together, confirming that the DLP printing process did not alter the emulsion droplet morphology (Figure 3c). Closer inspection revealed that the droplets are about 20–100 μm in diameter with slightly faceted surfaces. Individual spheres had very smooth surfaces, and the lack of contrast within each sphere suggested they were compositionally homogeneous.

We also studied the thermal stability and phase transitions of the 3D printed architectures by thermogravimetric analysis (TGA) and differential scanning calorimetry (DSC). The printed structures exhibited good thermal stability, with decomposition onset temperatures around 200 °C (Figure S6). Additionally, the DSC curves were consistent and reproducible across multiple heating-cooling cycles, displaying a single peak at 37 °C, corresponding to the isotropization temperature (T_{N-I}) of **5CB**, which retains the nematic mesomorphic order at room temperature (Figure S1). The thermomechanical properties of the printed structures were also characterized by dynamic mechanical analysis (DMA) (Figure S7). The storage modulus in the glassy state was found to be 200 MPa at 20 °C, corresponding

to the expected soft material properties for crosslinked LCs. Upon heating, the storage modulus decreased by around two orders of magnitude (from 200 MPa to 2 MPa) due to the loss of the LC properties of **5CB** upon phase transition from nematic to isotropic. The T_{N-I} was determined at the maximum of tan(δ), obtaining 34 °C, which is in good agreement with the value obtained by DSC.

Shape Memory Properties of the Printed Structures

Shape memory polymers are a class of smart, stimuli-responsive materials capable of undergoing controlled shape changes when exposed to external triggers.[19] Among them, thermoresponsive shape memory polymers exhibit a shape memory effect that is activated by temperature changes, typically in response to phase transitions. These materials can be temporarily deformed into a new shape, which remains stable until a specific temperature is reached, at which point the material reverts to its original form. This ability to reversibly switch between shapes makes shape memory polymers highly attractive for a wide range of
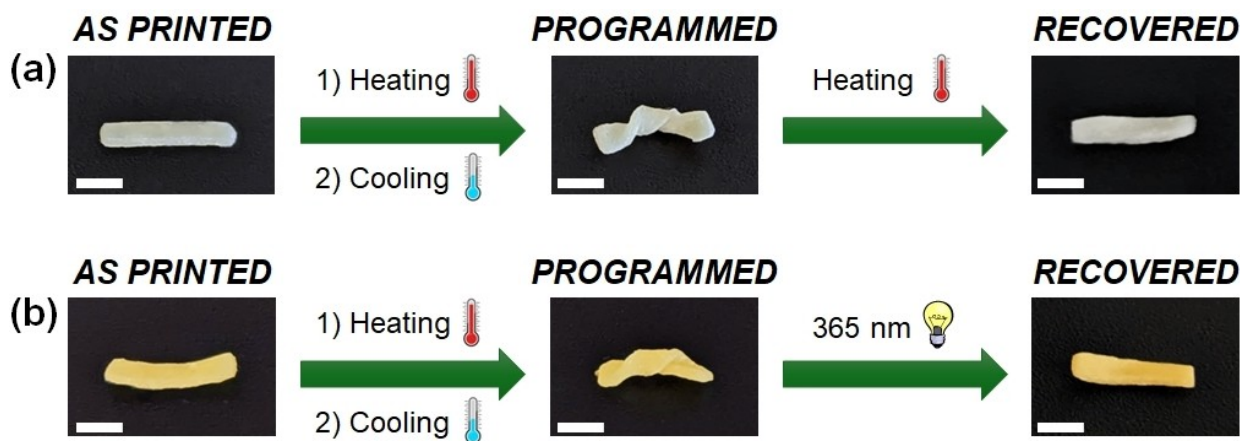
Figure 4. Shape memory tests (programming + fixation + recovery) using **(a)** temperature (75 °C) or **(b)** light irradiation (365 nm) for the recovery step. Photographs of the printed structures in their initial shape, temporary shape, and recovered shape. All structures were programmed at 75 °C and fixed at RT. Scale bar: 10 mm.

advanced applications, including aerospace technology, biomedical devices, flexible electronics, or soft robotics.

To evaluate the shape memory effect of the printed structures, the T_{N-I} is a key element in the design of the shape memory tests since it will determine the programming temperature (above T_{N-I}) and the fixation temperature (below T_{N-I}). The programming and recovery temperature was selected to be 75 °C to ensure that the material reaches to the isotropic state (above T_{N-I}). It is important to note, however, that the shape memory response can also occur at lower temperatures, albeit with a slower recovery rate. For fixation, the samples were cooled down to room temperature to "freeze" the programmed shape. The shape memory effect was evaluated using simple geometries consisting of 3D rectangular strips (15 mm×3 mm×1 mm), which were printed using the optimized formulation and printing parameters. Photographs of initial, programmed and recovered shapes are included in Figure 4a. To prove the repeatability of the shape memory effect, the same printed structure was used in three successive programming-fixation-recovery cycles without apparent loss of its initial properties and/or degradation, proving the excellent shape programming and recovery properties of the printed materials.

In addition to the inherent temperature response of the printed structures, we explored the incorporation of light-responsive behavior by embedding an organic dye as a photoabsorber in a post-printing step.[2a,7b] Specifically, an azobenzene dye (**AZO-C8** in Figure 5) was introduced by immersing the DLP-printed structures overnight in a dispersion of the dye in **5CB**. The successful integration of **AZO-C8** into the printed 3D structures was evidenced by a significant color change and confirmed by IR spectroscopy, which showed the appearance of the characteristic N=N and C–N stretching bands of azobenzene derivatives at 1453 cm^{-1} and 1138 cm^{-1}, respectively (Figure S8). DSC analysis revealed that this post-printing process did not alter the LC behavior of the material and resulted in a slightly higher T_{N-I} of 39 °C compared to the structure without
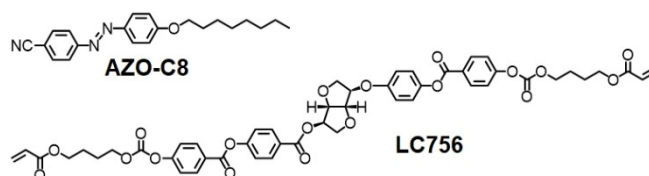
Figure 5. Chemical structure of azobenzene dye (**AZO-C8**) and chiral dopant crosslinker (**LC756**).

AZO-C8 dye (T_{N-I} = 37 °C) (Figure S9). The light-stimulated shape memory effect was investigated by programming the printed structures containing **AZO-C8**, deforming them while heating to 75 °C (above T_{N-I}), and then fixing the shape by cooling down to room temperature. Upon irradiation with 365 nm light, the deformed samples rapidly recovered their initial shape (Figure 4b). This process of programming, fixation, and light-stimulated recovery could be repeatable for at least three times without any noticeable change.

Formation of Intrinsically Porous 3D Structures

Structures with intrinsic porosity are highly desirable for applications such as gas separation, filtration, catalysis, and supporting 3D cell growth in tissue engineering. Preparing these systems is challenging due to the need to control numerous physical parameters, including mechanical properties, surface microstructure, texture, and porosity. To explore whether our methods could be extended to create intrinsically porous 3D structures, we extracted non-reactive **5CB** from the printed structures by washing it with an excess of dichloromethane (DCM), a solvent in which **5CB** is highly soluble. IR spectroscopy confirmed the successful extraction of **5CB** by the disappearance of the C≡N stretching band at 2226 cm^{-1} (Figure S4). DSC studies further validated the removal of **5CB**, as the printed structures, after washing with DCM, did not exhibit a nematic-to-isotropic transition,

unlike the structures prior to DCM washing (Figure S1). Similarly, DMA curves only displayed a phase transition at 64 °C, corresponding to the glass transition of the resulting polymer network without **5CB**, and did not show the T_{N-I} transition of **5CB** (Figure S6).

This alternative development process using DCM led to significant shrinkage ($\approx 60\%$) and a deformation of the 3D structures due to the complete removal of **5CB** (Figure 6), which accounts for approximately 80 wt % of the initial LC ink. Nonetheless, SEM analysis revealed that the 3D printed structures were composed of spherical droplets fused in an almost close-packed arrangement, but with a rougher surface due to the intrinsic porosity generated by the removal of **5CB** without significantly altering the overall emulsion droplet morphology (Figure 3d). The removal of **5CB** significantly impacted the shape memory effect, rendering the previously described three-step procedure of programming, fixation, and recovery unfeasible for the resulting 3D structures. However, we found that re-immersing the DCM-developed structure in **5CB** allowed for partial recovery of the original shape (Figure 6), thereby restoring some of the previously mentioned features and further demonstrating the intrinsic porosity of the material.

Fabrication of Reflective 3D Structures Based on Chiral Nematic LC Emulsions

To further demonstrate the versatility of our 3D printing method for LC emulsions, we expanded its application to include LC droplets containing a chiral nematic phase. Chiral nematic LCs, also known as cholesteric LCs, are soft photonic materials that exhibit selective light reflection due to their periodic helical supramolecular structure, where the pitch of the helix determines the wavelength of the reflected light.[13b,20] Typically, chiral nematic LCs are created by

Figure 6. Photographs of some printed structures at different stages: initial shape, DCM-washed shape, and **5CB**-inmersed (recovered) shape.

adding a chiral dopant to a nematic LC. For our experiments, we used a reactive chiral nematic mixture composed of non-reactive nematic **5CB**, mesogenic crosslinker **RM257**, chiral dopant crosslinker **LC756** (see chemical structure in Figure 5), and **BAPO** as photoinitiator. The color of the reflected light in our formulation can be precisely tuned by adjusting the concentration of the chiral dopant, specifically **LC756**. In this study, we prepared a green chiral nematic mixture by incorporating 3.5 wt % of **LC756**, resulting in a reflection wavelength of approximately 550 nm. DSC experiments confirmed that these reactive LC mixture remains in the chiral nematic LC phase at room temperature and transition to an isotropic phase at approximately 44 °C (Figure S10).

To prepare chiral nematic emulsion-based inks for DLP printing, we used the already described procedure, in which the reactive chiral nematic mixture was dissolved in DCM and emulsified using bulk emulsification techniques, resulting in LC droplets upon DCM evaporation. We employed a continuous phase containing **PVA** surfactant (0.1 wt %), **PEGDA** crosslinker (2.5 wt %), and **LAP** photoinitiator (0.25 wt %). **PVA** induced a radial helical orientation of the chiral nematic LC phase within the droplets, aligning mesogens parallel to the aqueous interface, as confirmed by POM. Under POM (Figure 7a), these droplets displayed a bright central spot due to the normal reflection of the chiral nematic organization, with several less-intense radial reflections corresponding to the photonic inter-droplet cross-communication.[21]

The chiral nematic emulsion-based ink proved to be printable, and we generated a Jacob's working curve at an intensity of 25 mW/cm^2 to determine optimal printing parameters (Figure S3). Compared to inks based on simple nematic LC emulsions, slight variations in the photopolymerization kinetics were observed. Having set the printing parameters, we evaluated the materials' 3D printability by fabricating simple and complex geometries with overhanging elements. For example, it was possible to print various 3D architectures such as a grid, a submarine, a sunflower, a rose, a rabbit, and an infinity ring with well-defined characteristics and remarkable surface quality (Figure 7c).

The as-printed structures did not exhibit vivid and well-defined colors, primarily due to light scattering caused by the difference in refractive indices between the chiral nematic LC droplets ($n \approx 1.6$) and the surrounding medium (i.e., air or water).[22] This mismatch leads to a broadening of the reflected light spectrum, which can mask the pure reflection colors typically associated with the selective reflection of chiral nematic LC droplets. However, under optical microscopy, we observed the characteristic reflection properties of the individual droplets within the 3D structures (Figure 7b). Each droplet displayed a reflective centered dot, attributed to the normal reflection of the chiral nematic organization, confirming that the chiral nematic arrangement remained intact after the 3D printing process. Future research will focus on matching the refractive index of the droplets with that of the embedding medium, which may mitigate the broadening of the reflection spectra and enhance color purity. Although our current 3D printing
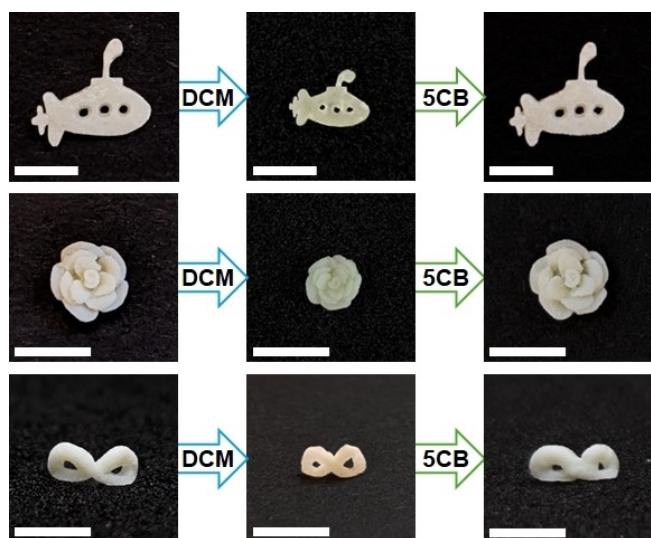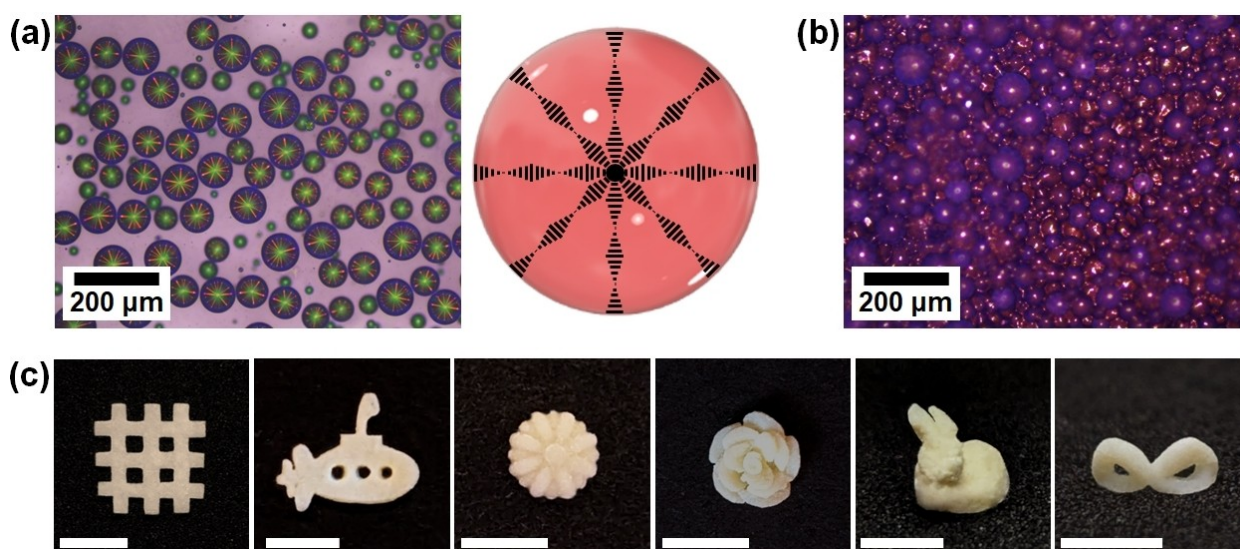
Figure 7. **(a)** Reflection-mode optical microscopy images of chiral nematic emulsions, and a schematic representation of the internal helical configuration. **(b)** Reflection-mode optical microscopy image of a 3D printed structure based on chiral nematic emulsions. **(c)** Photographs of 3D printed structures based on chiral nematic emulsions: grid, submarine, sunflower, rose, rabbit, and infinity ring (from left to right; scale bar: 5 mm).

approach was not compatible with alternative continuous phases such as quinoline (n ≈ 1.63)[22] or poly(methylphenyl)siloxane (n ≈ 1.52),[8f] further optimization of the system holds promise for overcoming this limitation and achieving more vibrant and precise reflection colors in future applications.

Conclusions

In conclusion, we have successfully developed a novel and versatile 4D printing approach using photo-polymerizable LC emulsions, demonstrating the ability to fabricate complex-shaped objects with advanced functionalities. The LC emulsion droplets were prepared via bulk emulsification using a reactive LC mixture containing non-reactive nematic LC (**5CB**) and a mesogenic crosslinker (**RM257**). By employing DLP printing, we achieved high-resolution production of intricate geometries while preserving the LC ordering from the precursor droplets. This retention of the LC arrangement endowed the printed materials with shape memory properties, enabling shape fixation and recovery in response to temperature changes. Additionally, the incorporation of an azobenzene dye in a post-printing step introduced light-responsive behavior into the shape memory properties, further enhancing the versatility of these smart materials.

We also explored the potential to create intrinsically porous 3D structures by selectively removing the non-reactive components from the printed geometries, thereby increasing the functional versatility of the printed objects. Furthermore, the successful integration of chiral nematic LCs into the emulsion droplets enabled the fabrication of 3D objects with tunable reflective properties, opening up new opportunities for photonic and optical applications.

Although our approach offers a versatile and effective method for manufacturing functional 4D structures, challenges remain, particularly in improving the color purity of reflective structures and refining the control over porosity. Nonetheless, this work represents the first reported example of DLP 3D printing with LC emulsions, paving the way for the development of 4D-printed structures based on smart, responsive materials with potential applications in adaptive optics, robotics, microfluidics, and biomedicine.

Acknowledgements

Conflict of Interest

The authors declare no conflict of interest.

Data Availability Statement

The data that support the findings of this study are available in the supplementary material of this article.

[1] a) C. A. Spiegel, E. Blasco, *Nature* **2024**, *627*, 276–277; b) Y. Zhang, Z. Dong, C. Li, H. Du, N. X. Fang, L. Wu, Y. Song, *Nat. Commun.* **2020**, *11*, 4685; c) S. C. Ligon, R. Liska, J. Stampfl, M. Gurr, R. Mülhaupt, *Chem. Rev.* **2017**, *117*, 10212–10290; d) D. Rus, M. T. Tolley, *Nature* **2015**, *521*, 467–475.

[2] a) P. Mainik, C. A. Spiegel, E. Blasco, *Adv. Mater.* **2024**, *36*, 2310100; b) S. A. M. Tofail, E. P. Koumoulos, A. Bandyopadhyay, S. Bose, L. O'Donoghue, C. Charitidis, *Mater. Today* **2018**, *21*, 22–37.

[3] M. Bodaghi, A. Zolfagharian, *Smart Materials in Additive Manufacturing, Volume 1: 4D Printing Principles and Fabrication*, Elsevier Science, **2022**.

[4] a) J.-Y. Wang, F. Jin, X.-Z. Dong, J. Liu, M.-L. Zheng, *Adv. Mater. Technol.* **2022**, *7*, 2200276; b) M. Champeau, D. A. Heinze, T. N. Viana, E. R. de Souza, A. C. Chinellato, S. Titotto, *Adv. Funct. Mater.* **2020**, *30*, 1910606; c) M. Hippler, E. Blasco, J. Qu, M. Tanaka, C. Barner-Kowollik, M. Wegener, M. Bastmeyer, *Nat. Commun.* **2019**, *10*, 232.

[5] a) C. A. Spiegel, M. Hackner, V. P. Bothe, J. P. Spatz, E. Blasco, *Adv. Funct. Mater.* **2022**, *32*, 2110580; b) M. P. Jeske, W. Zhang, M. Anthamatten, *Adv. Mater. Technol.* **2022**, *7*, 2101725; c) W. Zhang, H. Wang, H. Wang, J. Y. E. Chan, H. Liu, B. Zhang, Y.-F. Zhang, K. Agarwal, X. Yang, A. S. Ranganath, H. Y. Low, Q. Ge, J. K. W. Yang, *Nat. Commun.* **2021**, *12*, 112.

[6] a) S. Malekmohammadi, N. Sedghi Aminabad, A. Sabzi, A. Zarebkohan, M. Razavi, M. Vosough, M. Bodaghi, H. Maleki, *Biomedicine* **2021**, *9*, 1537; b) A. Terzopoulou, X. Wang, X.-Z. Chen, M. Palacios-Corella, C. Pujante, J. Herrero-Martín, X.-H. Qin, J. Sort, A. J. deMello, B. J. Nelson, J. Puigmartí-Luis, S. Pané, *Adv. Healthcare Mater.* **2020**, *9*, 2001031; c) H. Ceylan, I. C. Yasa, O. Yasa, A. F. Tabak, J. Giltinan, M. Sitti, *ACS Nano* **2019**, *13*, 3353–3362; d) X. Wang, X.-Z. Chen, C. C. J. Alcântara, S. Sevim, M. Hoop, A. Terzopoulou, C. de Marco, C. Hu, A. J. de Mello, P. Falcaro, S. Furukawa, B. J. Nelson, J. Puigmartí-Luis, S. Pané, *Adv. Mater.* **2019**, *31*, 1901592; e) J. Park, C. Jin, S. Lee, J.-Y. Kim, H. Choi, *Adv. Healthcare Mater.* **2019**, *8*, 1900213.

[7] a) L. Montesino, J. I. Martínez, C. Sánchez-Somolinos, *Adv. Funct. Mater.* **2024**, *34*, 2309019; b) L.-Y. Hsu, P. Mainik, A. Münchinger, S. Lindenthal, T. Spratte, A. Welle, J. Zaumseil, C. Selhuber-Unkel, M. Wegener, E. Blasco, *Adv. Mater. Technol.* **2023**, *8*, 2200801; c) S. J. D. Lugger, L. Ceamanos, D. J. Mulder, C. Sánchez-Somolinos, A. P. H. J. Schenning, *Adv. Mater. Technol.* **2023**, *8*, 2201472; d) P. Lyu, M. O. Astam, C. Sánchez-Somolinos, J. Liu, *Adv. Intell. Syst.* **2022**, *4*, 2200280; e) D. Martella, S. Nocentini, D. Nuzhdin, C. Parmeggiani, D. S. Wiersma, *Adv. Mater.* **2017**, *29*, 1704047; f) H. Zeng, P. Wasylczyk, C. Parmeggiani, D. Martella, M. Burresi, D. S. Wiersma, *Adv. Mater.* **2015**, *27*, 3883–3887; g) H.-Q.

Wang, Y. Tang, Z.-Y. Huang, F.-Z. Wang, P.-F. Qiu, X. Zhang, C.-H. Li, Q. Li, *Angew. Chem. Int. Ed.* **2023**, *62*, e202313728.

[8] a) C. Yang, Y. Xiao, L. Hu, J. Chen, C.-X. Zhao, P. Zhao, J. Ruan, Z. Wu, H. Yu, D. A. Weitz, D. Chen, *Small* **2023**, *19*, 2207073; b) S. Huang, Y. Huang, Q. Li, *Small Structures* **2021**, *2*, 2100038; c) Z. Zhu, J.-D. Liu, C. Liu, X. Wu, Q. Li, S. Chen, X. Zhao, D. A. Weitz, *Small* **2020**, *16*, 1903939; d) C. W. Visser, D. N. Amato, J. Mueller, J. A. Lewis, *Adv. Mater.* **2019**, *31*, 1904668; e) B. M. Rauzan, A. Z. Nelson, S. E. Lehman, R. H. Ewoldt, R. G. Nuzzo, *Adv. Funct. Mater.* **2018**, *28*, 1707032; f) A. Belmonte, M. Pilz da Cunha, K. Nickmans, A. P. H. J. Schenning, *Adv. Opt. Mater.* **2020**, *8*, 2000054.

[9] a) X. He, J. Wu, S. Xuan, S. Sun, X. Gong, *ACS Appl. Mater. Interfaces* **2022**, *14*, 9597–9607; b) M. J. Ford, C. P. Ambulo, T. A. Kent, E. J. Markvicka, C. Pan, J. Malen, T. H. Ware, C. Majidi, *PNAS* **2019**, *116*, 21438–21444; c) E. J. Markvicka, M. D. Bartlett, X. Huang, C. Majidi, *Nat. Mater.* **2018**, *17*, 618–624.

[10] a) J. S. Llorens, L. Barbera, A. F. Demirörs, A. R. Studart, *Adv. Mater.* **2023**, *35*, 2302868; b) A. F. Demirörs, E. Poloni, M. Chiesa, F. L. Bargardi, M. R. Binelli, W. Woigk, L. D. C. de Castro, N. Kleger, F. B. Coulter, A. Sicher, H. Galinski, F. Scheffold, A. R. Studart, *Nat. Commun.* **2022**, *13*, 4397; c) C. Yang, B. Wu, J. Ruan, P. Zhao, L. Chen, D. Chen, F. Ye, *Adv. Mater.* **2021**, *33*, 2006361.

[11] P. J. Collings, J. W. G. Goodby, *Introduction to liquid crystals: chemistry and physics*, 2nd ed., CRC Press, Boca Raton, Florida, **2019**.

[12] a) J. Uchida, B. Soberats, M. Gupta, T. Kato, *Adv. Mater.* **2022**, *34*, 2109063; b) T. Kato, J. Uchida, T. Ichikawa, T. Sakamoto, *Angew. Chem. Int. Ed.* **2018**, *57*, 4355–4371; c) H. K. Bisoyi, Q. Li, *Chem. Rev.* **2022**, *122*, 4887–4926.

[13] a) C. Tschierske, in *Chirality at the Nanoscale* (Ed.: D. B. Amabilino), Wiley-VCH Verlag GmbH & Co. KGaA, Weinheim, **2009**, pp. 271–304; b) L. Wang, A. M. Urbas, Q. Li, *Adv. Mater.* **2020**, *32*, 1801335.

[14] a) H.-Q. Chen, X.-Y. Wang, H. K. Bisoyi, L.-J. Chen, Q. Li, *Langmuir* **2021**, *37*, 3789–3807; b) D. S. Miller, X. Wang, N. L. Abbott, *Chem. Mater.* **2014**, *26*, 496–506.

[15] a) A. Terrel, S. Del Moral, A. Martínez-Bueno, A. Concellón, *Liq. Cryst.* **2024**, DOI: 10.1080/02678292.2024.2325587; b) A. Concellón, *Angew. Chem. Int. Ed.* **2023**, *62*, e202308857.

[16] a) Z. Guan, L. Wang, J. Bae, *Mater. Horiz.* **2022**, *9*, 1825–1849; b) C. A. Spiegel, M. Hippler, A. Münchinger, M. Bastmeyer, C. Barner-Kowollik, M. Wegener, E. Blasco, *Adv. Funct. Mater.* **2020**, *30*, 1907615.

[17] a) I. Dierking, *Adv. Mater.* **2000**, *12*, 167–181; b) I. Dierking, *Polym. Chem.* **2010**, *1*, 1153–1159.

[18] P. F. Jacobs, *Rapid prototyping & manufacturing: fundamentals of stereolithography*, Society of Manufacturing Engineers, **1992**.

[19] A. Lendlein, O. E. C. Gould, *Nat. Rev. Mater.* **2019**, *4*, 116–133.

[20] a) D. J. Mulder, A. P. H. J. Schenning, C. W. M. Bastiaansen, *J. Mater. Chem. C* **2014**, *2*, 6695–6705; b) J. Liu, Z.-P. Song, L.-Y. Sun, B.-X. Li, Y.-Q. Lu, Q. Li, *Responsive Mater.* **2023**, *1*, e20230005.

[21] a) J. Fan, Y. Li, H. K. Bisoyi, R. S. Zola, D.-k. Yang, T. J. Bunning, D. A. Weitz, Q. Li, *Angew. Chem. Int. Ed.* **2015**, *54*, 2160–2164; b) A. Concellón, D. Fong, T. M. Swager, *J. Am. Chem. Soc.* **2021**, *143*, 9177–9182; c) M. Schwartz, G. Lenzini, Y. Geng, P. B. Rønne, P. Y. A. Ryan, J. P. F. Lagerwall, *Adv. Mater.* **2018**, *30*, 1707382.

[22] E. Beltran-Gracia, O. L. Parri, *J. Mater. Chem. C* **2015**, *3*, 11335–11340.

Research Article

Polymer Chemistry

A. Concellón,* P. Mainik, C. Vazquez-Martel, C. Álvarez-Solana,
E. Blasco* —————————— e202421162

4D Printing of Liquid Crystal Emulsions for Smart Structures with Multiple Functionalities

- ✓ Shape Memory
- ✓ Intrinsic Porosity
- ✓ Reflective Properties
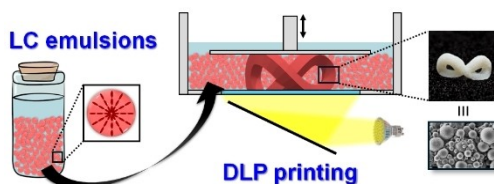
We present a novel 4D printing approach using digital light processing (DLP) to fabricate complex, multifunctional 3D structures from liquid crystal (LC) emulsions. This method preserves LC ordering, imparting tunable shape memory, light responsiveness, and porosity. The addition of chiral nematic LCs enables adjustable reflective properties, offering potential for applications in adaptive optics, robotics, and photonics.